Simulation of Gas Bremsstrahlung Radiation from APS Undulator Straight Sections using MARS[‡]

J. Dooling and L. Emery

Accelerator Systems Division, Advanced Photon Source, Argonne National Laboratory, 9700 S. Cass Ave. Argonne, IL 60439, USA

Abstract

We analyze the production of gas bremsstrahlung (GB) with regard to power, dose rate, and distributions. The contact dose behind a beam stop is simulated for stops fabricated from lead and tungsten. We compare the production of photoneutrons (PNs) from measurements and simulations. The beam stop dimensions necessary to shield a GB extremal ray are examined.

1. Introduction

A number of studies have been undertaken to quantify and measure the radiation produced at the APS and to specify the means necessary to mitigate its hazards. Specifically, APS Technical Bulletins (TB) and Light Source (LS) Notes [1,2,3,4] provide physical and engineering guidance regarding radiation source strength, material properties, and shielding requirements. Neutron fluences, measured in two undulator insertion device (ID) beamlines [5,6], 6ID and 11ID, are compared here with MARS simulations. MARS [7,8] is a group of freely available but closed source Monte Carlo programs used for the description of high-energy particle transport though matter. MARS is used to model the interaction of 7-GeV electrons in the APS storage ring (SR) with various forms of matter that may be encountered and the radiation resulting from those interactions. After a brief introduction in section one, the second section focuses on analysis of the gas bremsstrahlung (GB) source. Analytical, numerical, and empirical bremsstrahlung source descriptions are compared. In section three, earlier EGS4 results are given alongside recent MARS simulations estimating the dose in a tissue phantom in contact with a heavy-metal beam stop. MARS estimates of GB-induced, photoneutron production are compared with earlier measurements in section four. In section five, the first optics enclosure (FOE) geometry is modeled, and a method for calculating the extremal ray shielding requirement is described. MARS simulation results are summarized in section six. Throughout this document, error bars represent the standard deviation about the mean value.

2. Analysis

In the first part of this section we will compare the power and dose rate from gas bremsstrahlung (GB) photons calculated with an analytical formula, a MARS simulation, and a semi-empirical analysis [9] used in APS documents TB-20 [2] and LS-260 [10]. Some discrepancies are revealed. Next, we will check how well the MARS spatial photon distribution corresponds to analytical estimates.

The production of GB photons [11,12,13] can be determined from the radiative mass stopping power:

$$\left.\frac{dT}{dx}\right|_{rad} = -\frac{\rho T}{X_0}, \tag{1}$$

where T is the electron kinetic energy in MeV, and ρ is the mass density of the medium; in this regime, $T \approx E_o$, the total electron energy ($E_o = T + mc^2$). The radiation length is defined as

[‡] Work supported by U.S. Department of Energy, Office of Science, Office of Basic Energy Sciences, under Contract No. DE-AC02-06CH11357.

$$X_0^{-1} = 4\alpha r_e^2 \frac{N_A}{A^*} Z_{eff} \left(Z_{eff} + 1\right) \left[\ln\left(\frac{183}{Z_{eff}^{1/3}}\right) + \frac{1}{18} \right], \quad (2)$$

where X_0 is expressed in units of g/cm^2, N_A is Avagadro's number, the fine structure constant α=1/137, the classical electron radius r_e=2.83x10^{-13}cm, A* is the effective atomic mass described below, and Z is the atomic number [14,15]. Tsai [16] and Yao et al. [17] express the radiation length slightly differently but with virtually the same numerical results. The effective atomic mass of a gas mixture such as air is defined as a sum of the weighted molar fraction of the atomic mass of each component in the mixture,

$$A^* = \sum_i f_i A_i \ . \quad (3)$$

For the main constituents of air (N, O, and Ar) A*=14.66 g/mole. In a manner similar to that given by Eq. (3), the effective atomic number for air is determined as Z_{eff}=7.31. Given A* and Z_{eff}, the radiation length for air is found to be 37.06 g/cm^2. High-energy electrons will interact with the electrons and nucleus of individual atoms, not collectively with the molecules. Equation (1) expresses the photon energy loss per electron per cm and provides a convenient way to calculate the GB power. The total GB power is written as

$$P_\gamma \left\{ \frac{MeV}{s} \right\} = 1.7x10^{18} \frac{p\{nTorr\} I\{mA\}}{T_K\{K\}} \frac{\rho\left\{g/cm^3\right\}}{X_o\left\{g/cm^2\right\}} L_{ss}\{cm\} T\{MeV\}, \quad (4)$$

where I is the stored beam current, p is the residual gas pressure, T_K is the residual gas temperature, and L_{ss} is the total length of the straight section. The total GB power per mA from 7 GeV electrons in a residual background gas pressure of 1 nTorr air at 293K (20°C) is 4.28x10^{-7} W for a 1538-cm-long straight section. For all temperature-dependent calculations made here, it is assumed T_K=293K. Residual gas analysis (RGA) studies of gas composition in APS insertion device (ID) beamlines 6 and 11 indicated Z_{eff} values vary significantly [5,6]. A comparison of GB power levels, normalized to 1 nT and 1 mA, are given in Table 1. The MARS result is approximately 20 percent less than the analytical value; however, the measured GB power levels are low by factors of 3.8-24.

	Z_{eff}	*$P_{\gamma,meas}$ [5,10,18,19] (W/Torr/mA)*	*Analytic, Eq. (4) (W/nTorr/mA)*	*MARS (W/nTorr/mA)*
Air	7.3	(1.0x10^{-7})	4.28x10^{-7}	3.4x10-7
6-ID e$^-$	4.08	0.6±0.03x10^{-8}	1.46x10^{-7}	*1.16x10-7
10-ID e$^+$	4.6	1.0x10^{-8}	1.82x10^{-7}	*1.45x10-7
11-ID e$^-$	3.18	1.9±0.14x10^{-8}†	0.94x10^{-7}	*0.75x10-7

* MARS Air result scaled with Z_{eff}.

† Given as 2.9x10^{-8} W/nTorr/mA (118 GeV/s/nTorr/mA) in Ref. 5

Table 1 - Comparison of measured, predicted, and simulated normalized GB power.

No analytical estimates are given for GB power in Refs. 10 or 19. A semi-empirical dose prediction based on a flux-to-dose conversion factor is provided where the background gas is assumed to be air (see the discussion associated with Eq. (7)). The GB power used in LS-260 [10] comes from Rindi [14], but its quantity is only partially provided. An estimated level of 1.2x10^5 photons per second is mentioned for the beamlines in Refs. 10 and 19; however, the average photon energy is not given, nor are the conditions for

which the estimate is made (current or pressure). As discussed below, the average photon energy determined from the analytical GB spectral distribution is found to be 531 MeV. Assuming the estimated photon rate is made for 100-mA operation in an air background of 1 nTorr, the normalized GB power is $1.0\text{x}10^{-7}$ W/nTorr/mA. The estimated level is roughly a factor of 4 times lower than the analytical result presented in Table 1; this discrepancy has been noted elsewhere [20]. Now that the GB power is calculated, let us estimate the dose. Normally, one would continue to use a simulation program for this calculation. However, for the simple geometry described here, we can compare analytical and numerical results, as well as examine what people did in the past.

Using flux-to-dose conversion factors provided by Rogers [21], an estimate of maximum GB dose can be obtained once the photon flux and average photon energy are known. The GB photon spectral fluence was predicted by MARS for 300-mA, 7-GeV electrons striking a 24-cm length, 1-atmosphere (760 Torr, ρ_{air}=0.001205g/cm^3) air target. The total photon fluence is determined by integrating gamma spectral fluence over the energy range and multiplying this result with the cross-sectional area of the volume in which the photon spectrum is tallied. In MARS, the dose from photons in a given region is determined by integrating the spectral fluence with the energy-dependent flux-to-dose conversion factor [21,22]. For the dose calculation, a cross-sectional area of 1 cm^2 is used. We must scale for gas pressure (p_{ss}=1 nTorr) as well as for the straight-section length (L_{ss}=1538 cm). The average GB photon energy determined from the MARS spectrum over the energy range of 0.2 MeV to 7000 MeV, $\langle k_m \rangle$=356 MeV. In MARS output, the dose from photons in a given region is determined by integrating the spectral fluence with the energy-dependent flux-to-dose conversion factor [21,22]:

$$\dot{D}_{\gamma,\text{MARS}} = \int_{k_{min}}^{k_{max}} dk\, SPG(k) \cdot f_\phi(k); \tag{5}$$

however, here we want to follow the steps used in the analytical approach. Using the normalized power found in Table 1, the photon flux in 1 cm^2 per mA is just the GB power divided by the average energy per photon. The dose rate can be expressed as

$$\dot{D}_{GBm} = \frac{P_{GBm}}{\langle k_m \rangle} \frac{f_\phi(\langle k_m \rangle)}{A_{min}} I p, \tag{6}$$

where A_{min}=1cm^2. The value of $f_\phi(\langle k_m \rangle)$ was found by linear interpolation of Rogers' simulation data [21] (=$2.74\text{x}10^{-10}$ Sv cm^2). The analytical spectrum varies as 1/E, differing from that of the simulation at low energy. MARS indicates a modest enhancement of the low-energy photon spectrum. Integrating over the same energy range, the average analytic photon energy $\langle k_a \rangle$ = 531 MeV. Using the power level defined in Eq. (4), the analytic dose rate is determined using the same form as Eq. (6), replacing $\langle k_m \rangle$ with $\langle k_a \rangle$. The value of $f_\phi(\langle k_a \rangle)$ is again interpolated from Rogers' data (=$3.22\text{x}10^{-10}$ Sv cm^2). Finally, a semi-empirical, total beam-integrated GB dose rate was used to determine the source term for the EGS4 simulations and is expressed as [9]

$$\dot{D}_{se} = \frac{f_\Gamma \Gamma L_{ss}}{\pi \theta_{gb}^2 X_o L (L + L_{ss})}, \tag{7}$$

where f_Γ is another effective flux-to-dose conversion factor for bremsstrahlung photons [10,19] (f_Γ=3×10^{-6} Gy/hr/Γ), Γ is the number of electrons per second (300 mA=1.873×10^{18}e/s), L_{ss} is the length of the ID straight section, $\theta_{gb}=1/\gamma$ is the characteristic opening angle of the radiation cone ($1/1.37\times10^4$=73 μrad), X_o is the radiation length in air for 1 nTorr (37.1 g/cm^2/ρ_{1nTorr}=2.35×10^{16}cm), and L is the length from the end of the straight section to the observation point (2440 cm). Comparison of initial dose rates are given in Table 2. The MARS GB power is 20 percent lower than that from the analytic model; however, the two dose results differ by less than 1 percent owing to the difference in average energy.

The dose rate given by Eq. (6) relies on the integration of the MARS photon spectal fluence to determine the total power and average photon energy. With these quantities, the dose rate is calculated manually using the flux-to-dose conversion factor just described; this is referred to as the MARS spectral fluence result in Table

2. The dose rates for this and the analytical case are determined assuming that all the GB power is intercepted by a 1-cc target volume defined by $r=1/\sqrt{\pi}$ cm and that the dose is uniform throughout this volume. In reality, neither of these assumptions are true. The dose will spread out beyond the boundaries of the target volume, especially at the downstream (DS) end of the phantom where the maximum dose is obtained. The GB transverse beam distribution, however, is still relatively narrow. The dose within the FWHM radius r_{FWHM} is much higher than that of the 1-cc cylinder. Assuming the radius of the GB beam at the output of the straight section is $\theta_{gb}L_{ss}$ yields 0.112 cm; this increases to 0.293 cm at the DS end of the phantom. The MARS simulation yields r_{FWHM}=0.267 cm at the DS end of the phantom. Using the simple model given by Eq. (6) (all GB power contained within the angular cone), the dose calculated at the source will be the same as that at the DS end of the phantom, since in both cases the radii of the GB is less than $1/\sqrt{\pi}$. We are ignoring any showering or absorption in the phantom. When considering the dose from GB radiation, a 1-cc volume can be employed but should more accurately reflect the transverse beam size. Rather than arbitrarily using a cylinder where $2r\approx1$ cm or a 1-cm cube, a more pertinent geometry would be a cylinder where the radius is defined by the width of the beam, such as r_{FWHM}. In the present case where the simulation predicts r_{FWHM}=0.267 cm, the length of the cylinder becomes $1\ cm^3/(\pi[0.267\ cm]^2)$=4.47 cm. The 1-cc volume now takes on the dimensions of a short drinking straw. Employing this criterion, the analytical and MARS fluence calculations via Eq. (6) both yield dose rates of approximately 6.5 Sv/hr; the full MARS simulation, which accounts for beam spreading and absorption, indicates 3.1 Sv/hr. The semi-empirical formula takes spreading into account via distance from the source [23].

Method	Analytic source $r=1/\sqrt{\pi}$ (r=0.293 cm)	MARS spectral fluence $r=1/\sqrt{\pi}$ (r=0.293 cm)	Semi-empirical	MARS direct $r=1/\sqrt{\pi}$ (r=0.267 cm)
$\dot{D}_r$ (Sv/hr)	1.75 (6.48)	1.76 (6.52)	2.23	0.70 (3.13)

Table 2 - Maximum GB dose rate estimates in a 1-cc cylindrical volume where the cross sectional area is 1 cm^2. The first two values in parentheses assume full power within the FWHM volume; whereas the MARS direct value refers to the peak dose within the simulation FWHM volume and thus accounts for beam spreading and absorption. The maximum dose rates are estimates at the DS end of the FOE phantom without any shielding present. No geometrical effect is evident for the semi-empirical estimate.

The GB transverse spatial distribution is examined at the location of a beam stop, 31 m downstream of the center of the undulator straight section. A linear y-profile of the bremsstrahlung photon flux obtained from a 10^{th} order polynomial fit to the integrated data is shown in Figure 1. The beam width is in reasonable agreement with the opening angle approximation $2L\theta_{gb}$=4.52mm (L=31 m). One would like to know if the 1-atm, 24-cm-long air target used to generate the GB radiation leads to an accurate description of the GB photon beam or does multiple scattering broaden the distribution. GB generated by scattered electrons will possess a portion of the angular deviation of the electron. The angular width of the GB radiation cone may be expressed as a quadrature sum of the intrinsic thin-target GB opening angle with a function of the electron scattering angle expressed as $\Theta^2_{GB}=\theta^2_{gb}+f^2(\Theta_{rms})$, where for high-energy electrons [7] $\Theta_{rms}= E_s/T\sqrt{(2x/X_o)}$ (projected distribution), x is the distance in radiation lengths these particles travel through the target medium, and $E_s=\sqrt{(4\pi/\alpha)}m_ec^2$ =21.2 MeV. The projected rms electron angle is Θ_{rms}=59.7 μrad for 7 GeV. Our hypothesis is that electrons scatter once through the gas, and thus the rms electron angle may not be given accurately by the above thin-target formula. A simple model is chosen for $f(\Theta_{GB})$, namely $f(\Theta_{rms})=k_{gb}\Theta_{rms}$, where k_{gb} is a constant to be determined from MARS simulations. From Fig. 1, the total opening angle [24] is $\Theta_{GB}=5.07x10^{-3}m/2L$=81.8 μrad; the value of k_{gb} is calculated to be k_{gb}=0.62. This suggests that scattered electrons in the air target are contributing to the angular width of the GB beam. If k_{gb} was zero, then this would be an indication that there was at most one scattering of the electrons. If k_{bg} was 1, multiple scatterings of electrons would be taking place in the air target. The effect is modest, but clearly limits the degree to which the air target pressure or length could be increased to improve simulation statistics. Thus we keep the air target model of 1 atm, 24 cm for the rest of the analyses.

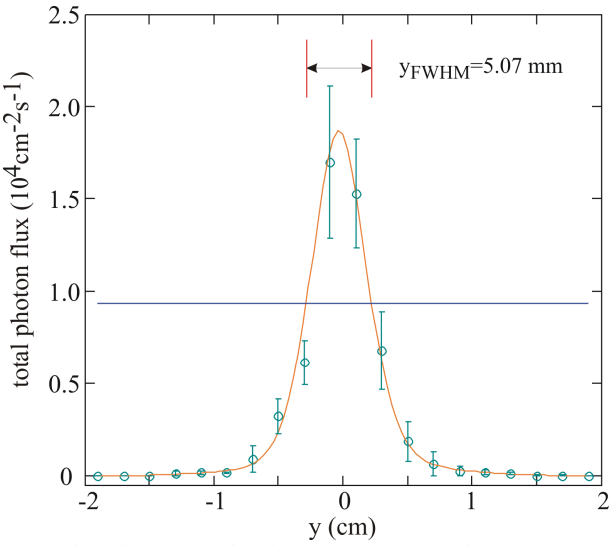

Fig.1 - MARS GB y-distribution and polynomial fit 31 m downstream of the air target.

3. Contact Dose

MARS is used to compare the dose levels reported in TB-20 [2] from simulations using EGS4. The EGS4 calculation did not account for the production of photoneutrons (PNs) in the target, and an arbitrary factor of 2 was used to include the neutron contribution to total dose. In all cases presented here, the production of PNs is included in MARS results. In the MARS simulation 300 mA of electrons at an energy of 7.0 GeV is used to generate the GB beam. In the simulation, the thickness of the target shield block was varied from 1 to 30 cm. The simulation dose was recorded in a tissue phantom, 20 cm by 20 cm in transverse dimensions and 30 cm in depth, in contact with the beam stop. The minimum volume employed in the analysis is 1 cm^3. MARS is set up to provide histograms in Cartesian coordinates; however, we expect the radiation dose, 3-D profile to have cylindrical symmetry. We need to generate an r-z distribution from MARS data to find the maximum dose. This is done by Abel inversion (AI) of x-z or y-z histogram average dose data [25]. The radial density (dose) can expressed as

$$f(r,z) = -\frac{L_y}{\pi}\int_r^a \frac{dF(x,z)}{dx}\frac{dx}{\left(x^2 - r^2\right)^{1/2}}, \tag{8}$$

where a is the radial boundary of the dose rate profile; and F(x,z), given in units of mSv/hr, is the y-averaged, x-z dose rate obtained from MARS across the y-thickness of the phantom L_y=20 cm. The AI technique requires the line density, which is obtained by taking the product of the average dose F(x,z) and L_y. Note that because of symmetry, the radial profile can equally be expressed in terms of the x-integrated dose rates by swapping x with y in Eq. (8). Equation (8) has to be evaluated at $z=z_{max}$, i.e., the z position where the dose is maximum. When a stop is present, even for the minimum thickness simulated (1cm), z_{max} is located at the upstream end of the phantom in the z-section adjacent to the beam stop. We make the assumption that the peak dose occurs at x=0, the center of the phantom.

TB-20 and the MARS AI method are compared in Figure 2. At 10 cm, the maximum dose predicted with the EGS4 analysis is approximately twice that from MARS for peak dose in 1 cc. This result is puzzling since both simulations use similar physics in this region where the electromagnetic shower dominates the dose rate. Comparing MARS and EGS4 output for stop thicknesses up to 30 cm, the attenuation of dose rate in the photon-dominated regions are approximately the same, as shown Figure 3. For thicker targets however, the dose rate no longer follows photon attenuation, as PNs begins to dominate. At the time the EGS4 simulations were conducted for TB-20, neutron contributions were not included in the dose. To account for the missing neutrons, the authors of TB-20 assumed that neutrons were responsible for half the dose and thereby lowered the dose rate limits by a factor of 2. For comparative purposes, the lowered dose rate limit of 1.25 μSv/hr is indicated in both Figs. 2 and 3.

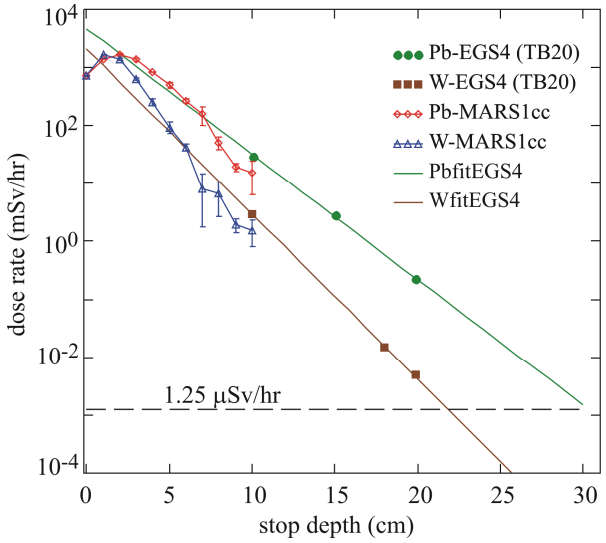

Fig.2 - Maximum dose from MARS in 1 cc and EGS4 from TB-20 for Pb and W stop thicknesses.

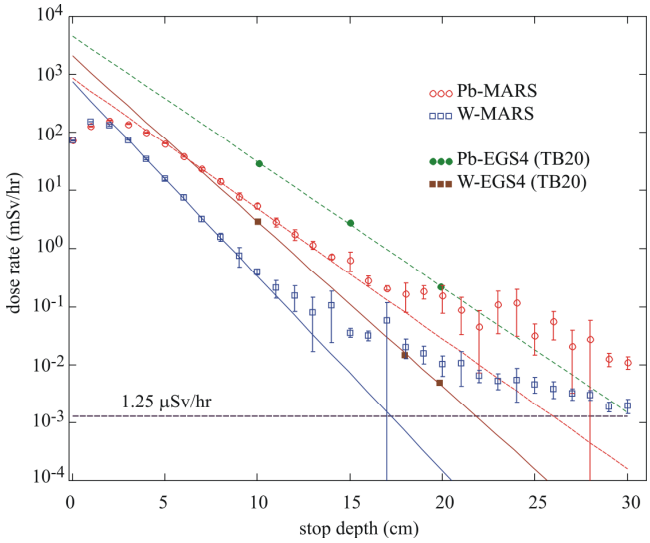

Fig.3 - Maximum MARS phantom dose (4x4x5 cm^3 element) and EGS4 dose for Pb and W stop thicknesses. Exponential fits for EGS and MARS data are given in the photon-dominated dose regions. Dashed lines compare results in Pb and the solid, in W.

The mass attenuation coefficients for Pb and W are given in Table 3. The coefficient of the exponent should approximately represent the minimum mass attenuation coefficient for each metal. These coefficients are compared with minimum mass attenuation values given by Hubbell [26] which occur near 4 MeV for both Pb and W.

	μ/ρ (4 MeV) (cm^2/g)	μ/ρ EGS4 (cm^2/g)	μ/ρ MARS (cm^2/g)
Pb	0.0420	0.0439	0.0456
W	0.0404	0.0341	0.0401

Table 3 - Mass attenuation coefficients for Pb and W comparing EGS4 and MARS with min. attenuation near 4 MeV.

4. Photoneutron (PN) Production

A study of PN dose resulting from GB [10,19] striking thick targets of various materials was conducted by Pisharody et al. [5,6]; specifically, the materials examined were Cu, Fe, W, and Pb. A comparison of these data with MARS simulations is presented here to evaluate its ability to simulate PN dose. In Refs. 5 and 6, an Andersson-Braun (AB) remmeter was used to measure the PN dose. The plan geometry of the MARS simulation is presented in Figure 4; in this case, an iron target receives the GB beam. The simulation dose is again recorded in a tissue phantom, 20 cm by 20 cm in transverse dimensions (y and z) and 30 cm in depth (x), relative to the incident beam.

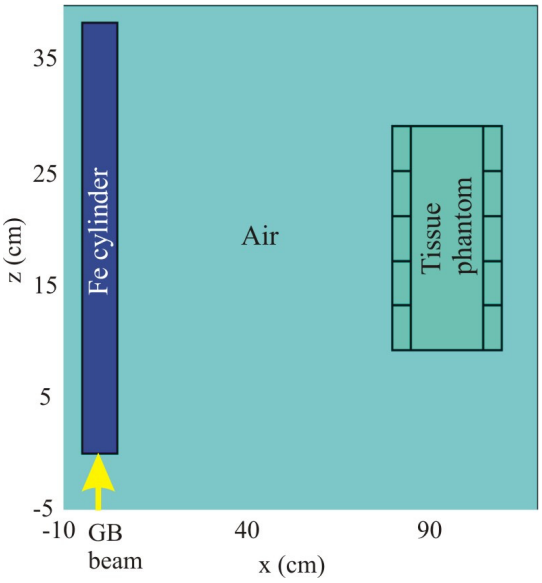

Fig.4 - Plan geometry of the MARS PN measurement simulation.

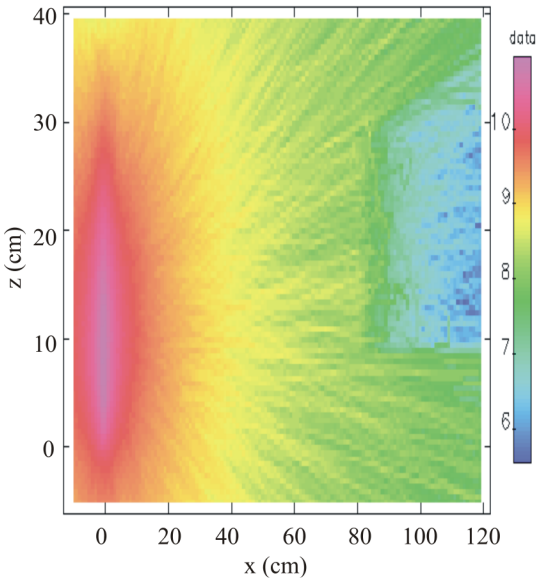

Fig.5 - Contour plot of uncorrected MARS PN dose from an APS GB beam striking the Fe target shown in Fig. 4. Dose is presented on a log scale.

In Fig. 5, a contour plot of the PN dose predicted by MARS is shown for the geometry given in Fig. 4. The simulation results presented in Fig. 5 must be normalized for the actual pressure and current as mentioned above. PN dose results from measurements given in Refs. 5 and 6, and scaled MARS simulation output are presented for comparison in Table 4. The PN measurements presented in Table 4 are obtained from beamlines 6-ID and 11-ID. For 6-ID, the measured PN dose rate for Fe is the average for the two highest current levels (93.4 and 92.7 mA) in Table 6 of Refs. 5 and 6, likewise for Cu and W, and from the highest current for Pb. For 11-ID, the measured PN dose rate for Fe is the average of the three highest current levels (96.6, 93.3, and 90.2 mA) in Table 5 of Refs. 5 and 6, likewise for Cu, but the lowest three for W and Pb. Target dimensions are varied to maintain lengths of $20X_o$ and widths of $6X_o$. The dose rates given in Table 4 for beamline 6-ID are approximately 3-5 times larger than the measured values; whereas those given for beamline 11-ID are much closer. Several possibilities exist that may explain the differences in the two sets of results: 1) Residual gas Z_{eff}. The actual Z_{eff} values in undulator beamlines are difficult to definitively ascertain. 2) Residual gas pressure. Pressure is another parameter that can vary from beamline to beamline. The Z_{eff} quoted for 11-ID is 3.18, yet the GB power from this line is 3-4 times higher than that of 6-ID. This suggests that the pressure or other factors may be considerably different for these two lines. 3) Beam pipe misalignment. Prior to the installation of an ID in the 6-ID undulator straight section, but after the GB measurements had been made, a 1-mrad bend in beam central orbit trajectory was noted through this region. The misalignment may have reduced the GB power by a factor of 3 in 6-ID.

Beamline	6-ID				11-ID			
Target Material	Fe	Cu	W	Pb	Fe	Cu	W	Pb
I (mA)	93.1	90.1	88.5	76.1	93.4	92.2	78.4	76.2
P (nT)	9.69	9.41	9.29	8.22	8.97	8.88	7.78	7.54
AB Remmeter (μSv/hr)	0.150	0.130	0.186	0.177	0.371	0.462	0.393	0.425
MARS (μSv/hr)	0.674	0.665	0.526	0.525	0.406	0.417	0.254	0.313

Table 4 - Comparison of PN dose measurements made in Refs. 5 and 6 for beamline 6-ID and 11-ID with MARS simulations correcting for Z_{eff} between air (7.3) used in MARS and a measured values of 4.08 (6-ID) and 3.18 (11-ID).

5. First Optics Enclosure (FOE) Study

Simulation studies have been conducted with MARS to assess shielding requirements. In the first study, dose levels in contact with the outside wall of the FOE are examined when GB radiation strikes a Pb beam-stop within the FOE. In the second study, the thickness of lead required to shield against the GB extremal ray is determined. For brevity, only the results of the second study are mentioned here. The FOE Pb shielding thicknesses used are 19 mm for the outside wall, 50 mm plus an additional 50 mm by 1-m^2 sheet centered on the beamline for the back wall, and 12 mm for the roof.

In the second task, dose from GB radiation striking a thick target scatterer within a beam pipe is simulated to compare with a similar analysis given in TB-20 to determine the extremal ray requirement. The geometry used for the new study described here is simple and obtained by replacing the square cross-section beamstop with a cylinder of the same length, 30 cm. The radius of the Pb target is varied while dose is recorded using the back-wall tissue phantom. Each data point is the average of ten MARS runs with 5×10^8 events per run representing the 7-GeV, 300-mA electron beam. The GB beam size was provided in Fig. 1. For the smallest target radii, a fraction of the primary GB beam passes by the target altogether (or perhaps experiences one scattering within the Moliere radius) and directly strikes the Pb shielding on the back wall. A fraction of this radiation then showers through the shielding to the back-wall phantom. Dose in the back wall phantom as a function of target radii is shown in Figure 6. For radii of 3 cm and above, primary bremsstrahlung is essentially blocked. Dose in the phantom varies weakly with target radius for r>3 cm.

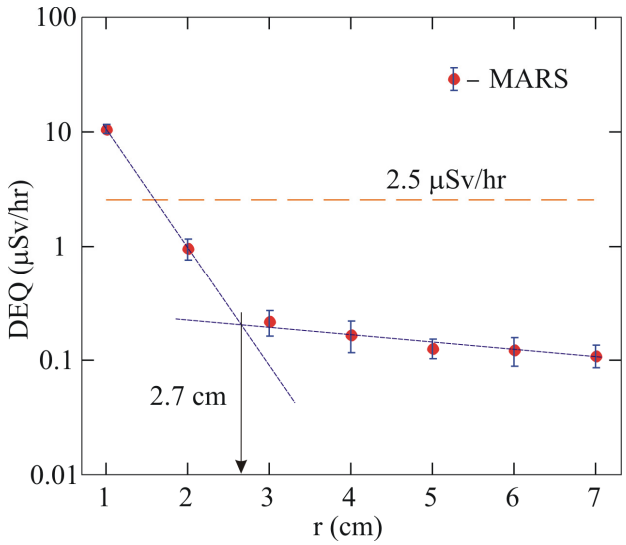

Fig.6 - Back-wall phantom dose versus beam target radius. The intersection of the fast and slow response curves represents the minimum radius of the Pb stop required to fully shield the back-wall phantom from direct GB radiation.

The dose in the phantom appears to be characterized by two behaviors: 1) a large variation with radius for small target dimensions and 2) a much smaller change for larger radii. The small radius dose appears to be the result of direct primary GB on the FOE back wall, as well as scattering up to the Moliere radius. The Moliere radius, the characteristic transverse dimension of the shower, may be written as [17] $X_m=X_oE_s/E_c$, where E_s was defined in Section 2, and the critical energy may be expressed as $E_c(\text{MeV})=800/(Z+1.2)$. The critical energy in Pb is 9.6 MeV, the radiation length is 5.8 g/cm^2, and the Moliere radius is 12.8 g/cm^2. In terms of physical length, the Moliere radius=X_m/ρ_{Pb}=1.1 cm. Assuming the beam edge radius r_e to be twice the FWHM value given in Fig. 1, then r_e=2(0.507 cm)=1.14 cm. The extremal distance r_{ed} is taken to be the difference between the back-wall phantom dose breakpoint radius r_{bp} and the beam-edge radius $r_{ed} = r_{bp} - r_e$. As shown in Fig. 6, r_{bp} = 2.7 cm; thus, r_{ed} = 1.56 cm ≈ 1.6 cm. Relative to the Moliere radius, the separation thickness is 1.6 cm/1.1 cm=1.45≈1.5; therefore, the separation between the extremal ray and the edge of the shielding is 1.5 X_m. In the context of TB-20 therefore, an extremal ray should come no closer than 1.6 cm to the lateral edge in Pb. For W with a Moliere radius of 0.65 cm, a similar argument sets the extremal ray shield edge separation at 0.98 cm≈1.0 cm. TB-20 [2] recommended that the extremal ray in the case of bremsstrahlung ray-tracing should not be closer than 4.5 cm from the lateral beamstop edge in Pb and 3.0 cm in W. The extra thickness in TB-20 provides additional protection, but specifications may need revisiting.

6. Discussion and Summary

GB power predicted by MARS in terms of the initial dose rate agrees to within 20 percent of the analytical model, see Table 1. Given the two independent methods employed, one should conclude that MARS does reasonably well simulating GB power. However, analysis and simulation both are significantly higher than the measured GB power. Possible explanations for the discrepancy were presented in Section 4 and include uncertainty in beamline Z_{eff}, pressure, and undulator straight section alignment. MARS does a good job reproducing the GB spatial distribution (see Fig. 1) in agreement with thin-target GB theory. Care must be taken, however not to make the air target too thick. An air-target pressure of 1 atmosphere and length of 24 cm appears to be an upper limit. Comparison of initial maximum dose rates predicted by MARS and the analytical model show good agreement; in addition, similar results are obtained with EGS4 in TB-20; however, an important difference is noted. The maximum dose from TB-20 appears conservative in the photon-dominated shower regions of the stops; however, this is not the case for thick stops. In the latter circumstance, dose comes primarily from photoneutrons. The Abel inversion method provides an accurate estimate of dose provided that statistics in the average dose profiles are good and the profiles are well behaved.

As for comparisons with PN measurements, MARS simulation results presented in Table 4 are approximately 4-5 times the measured values in beamline 6-ID and very close to that measured in 11-ID. Given the variability in the measured GB power due to fluctuations in Z_{eff} and pressure, MARS performs well. In addition, the MARS simulation work shows that, in order to properly model the PN dose, an accurate measure of undulator beamline Z_{eff} and pressure are necessary. As with the GB power mentioned above, the simulated PN dose levels generally exceed measured results.

An alternative method for determining the extremal ray thickness was used with MARS relative the approach taken in TB-20. By varying the radius of a cylindrical Pb target and calculating the dose in the back-wall phantom, one could observe the thickness where the direct and Moliere-scattered GB radiation was effectively turned off. The beam-edge radius of 1.1 cm and a dose break point radius of 2.7 cm indicates that 1.6 cm of Pb as an extremal ray thickness should be sufficient. The simulations indicate an additional thickness of 1.5 X_m should be sufficient to shield the extremal ray determined from ray-tracing.

References

[1] N. Ipe, D.R. Haeffner, E.E. Alp, S.C. Davey, R.J. Dejus, U. Hahn, B. Lai, K.J. Randall, and D. Shu, "Guide to Radiation Beamline Shielding Design at the APS," ANL/APS/TB-7 (1993).

[2] P. K. Job, D. R. Haeffner, and D. Shu, "Bremsstrahlung Scattering Calculations for the Beam Stops and Collimators in the APS Insertion-Device Beamlines," ANL/APS/TB-20 (1994).

[3] W. Yun et al., "Radiation Shielding of Insertion Device Beamlines Using a Mirror as the First Optical Element," ANL/APS/TB-21, February 1995.

[4] P. K. Job et al. "Guidelines for Beamline and Front-End Radiation Shielding Design at the Advanced Photon Source," ANL/APS/TB-44, Rev. 3, September 2008.

[5] M. Pisharody, E. Semones, and P. K. Job, "Dose Measurements of Bremsstrahlung-Produced Neutrons at the Advance Photon Source," ANL/APS/LS-269 (1998).

[6] M. Pisharody, E. Semones, and P.K. Job, Nucl. Instrum. Methods A, 430, 542 (1999).

[7] N. V. Mokhov and S. I. Striganov, "MARS15 overview," Technical Report Fermilab-Conf-07/008-AD, 2007.

[8] N. V. Mokhov et al., "Physics models in the MARS15 code for accelerator and space applications," in Int. Conf. on Nuclear Data for Science and Technology, AIP Conf. Proc. 769, 1618-1623 (2004).

[9] J. C. Franck, "Bremsstrahlung du Faisceau Stocke sur les molecules Residuelles de la Chambre Avide de Suder ACO," LURE EP 88–01 (1988).

[10] M. Pisharody, P. K. Job, S. Magill, J. Proudfoot, and R. Stanek, "Measurement of Gas Bremsstrahlung from the Insertion Device Beamlines of the Advanced Photon Source," ANL/APS/LS-260, March 1997.

[11] H. W. Koch and J. W. Motz, Rev. Mod. Phys. 31(4), 920 (1959).

[12] W. R. Nelson, "Properties of the EM Cascade," SLAC-PUB-4203, February 1987.

[13] J. C. Liu, W. R. Nelson, and K. R. Kase, Health Physics 68(2), 205 (1995).

[14] Rindi, Health Physics 42, 187 (1982).

[15] G. Tromba and A. Rindi, Nucl. Instrum. Methods A 292, 700 (1990).

[16] Y.-S. Tsai, Rev. Mod. Phys. 46(4), 815 (1974)
[17] W.-M. Yao et al., Journal of Physics G 33, 1 (2006).
[18] P. K. Job, M. Pisharody, E. Semones, Nucl. Instrum. Methods A 438, 540 (1999).
[19] M. Pisharody et al., Nucl. Instrum. Methods A 401, 442 (1997).
[20] Y. Asano et al., Nucl. Instrum. Methods A 451, 685 (2000).
[21] D. W. O. Rogers, Health Physics 46(2), 891(1984).
[22] ICRP Pub. 51, "Data for Use in Protection Against External Radiation," Annals of the IRCP, 17(2/3), Pergamon, New York, 26 (1987).
[23] Y. Asano and N. Sasamoto, Radiation Protection Dosimetry 82(3), 167 (1999).
[24] H. J. Moe, "Radiological Considerations for the Operation of the Advanced Photon Source Storage Ring – Revised," ANL/APS/LS-295 (1997).
[25] H. Hutchinson, Principles of plasma diagnostics, Cambridge, New York, 1987, p. 124.
[26] J.H. Hubbell, NSRDS-NBS 29, August 1969.